

**Abstract.** We present times series of high resolution spectra of AGB variables at  $4\mu\text{m}$ . Line profiles from the major contributors to the spectra of oxygen rich stars at  $4\mu\text{m}$ , OH,  $\text{H}_2\text{O}$ , HCl and SiO, are examined. The velocity as well as shape variations of these profiles with time are discussed. The line profiles investigated frequently have emission and multiple absorption components. The changes with time of the  $4\mu\text{m}$  region lines do not always follow the cyclic variability seen in NIR spectra and in the photometric light curve. We interpret and discuss the results qualitatively considering comparing the spectral variability with that of the well behaved  $1.6\mu\text{m}$  region and of dynamical model atmospheres. Miras and semiregular variables are compared. The origins of non-periodic behavior are discussed, including the role of spatial inhomogeneities in the stellar atmosphere.

**Key words:** stars: variables: general – stars: late-type – stars: AGB and post-AGB – stars: atmospheres

# $4\ \mu\text{m}$ spectra of AGB stars I. Observations

T. Lebzelter<sup>1</sup>, K.H. Hinkle<sup>2</sup>, and B. Aringer<sup>1</sup>

<sup>1</sup> Institut für Astronomie, Universität Wien, Türkenschanzstr. 17, A-1180 Vienna, Austria

<sup>2</sup> Kitt Peak National Observatory, National Optical Astronomy Observatories \*, 950 N.Cherry Avenue, P.O.Box 26732, Tucson, Arizona 85726

Received / Accepted

## 1. Introduction

The structure of the envelopes of Asymptotic Giant Branch (AGB) stars is dominated by large amplitude stellar pulsations. The mechanical energy of the pulsation can be larger than  $L/c$  by orders of magnitude (Hinkle et al. 1982), resulting in a cool, highly extended outer atmosphere. As a result of the pulsational flow of mechanical energy, the structure of the atmosphere varies strongly during the light cycle. It is possible with time series spectra to monitor the flow of material in the stellar atmosphere. In addition, velocities measured from different spectral transitions of different atomic and molecular species probe the dynamics at different (optical) depths in the atmosphere.

One result of the extended, cool atmosphere of these stars is that the stellar flux is primarily emitted in the infrared. Due to the rich infrared molecular spectra of the cool AGB stars, the infrared is also the optimum spectral region for studying the outer atmosphere of these stars. The analysis of time series of high resolution infrared spectra has been used over three decades by Hinkle and collaborators (e.g. Hinkle et al. 1982, 1984, 1997). Both miras and the lower amplitude semiregular variables have been investigated. The authors mainly used CO lines in the  $1.6\text{--}2.5\ \mu\text{m}$  region, since those transitions can be easily identified and observed. The high excitation first overtone CO lines and the second overtone lines of CO show velocity variations of  $25$  to  $30\ \text{km s}^{-1}$  in miras and about  $10\ \text{km s}^{-1}$  and less in semiregular variables. In the  $1.5\text{--}2.5\ \mu\text{m}$  region other atomic and molecular lines have been found to have similar behavior, while low excitation first overtone lines of CO show only very small velocity changes with phase. It has been suggested that these spectral lines as well as some of the  $\text{H}_2\text{O}$  lines probe a more extended pseudo-stationary layer. Spectral lines with excitation potentials near zero volts and large column densities, e.g. the lowest excitation CO fundamental lines situated around  $4.6\ \mu\text{m}$ ,

probe the classic, expanding circumstellar shell (Ryde et al. 2000).

In this paper we will investigate the molecular spectra in the  $4\ \mu\text{m}$  region. In oxygen rich atmospheres, the principal molecular constituents are the first overtone SiO bands, the fundamental bands of OH, and the HCl fundamental. In addition, the  $4\ \mu\text{m}$  region is blanketed by a large number of weak water lines in stars with  $\text{O} \gg \text{C}$ . We will discuss high spectral resolution observations of lines from all four of these molecules in this paper. This is the first use of these  $4\ \mu\text{m}$  lines at high resolution for monitoring the atmospheric changes in pulsating stars. However, the  $4\ \mu\text{m}$  spectrum of SiO has been monitored previously at medium and low resolution (Hinkle et al. 1976; Rinsland & Wing 1982).

Aringer et al. (1997, 1999b) have shown from medium resolution  $4\ \mu\text{m}$  spectra that using hydrostatic models cannot reproduce the spectra properly. In order to match the observations one needs to introduce additional features like the “warm molecular envelope” proposed by Tsuji et al. (1997). On the other hand, calculations based on recently developed dynamical atmospheric models (Höfner et al. 1998) have the ability to reproduce the observed spectral features as shown by Aringer et al. (1999b) for the SiO first overtone band heads around  $4\ \mu\text{m}$ . In this paper we will present the observational data for a sample of miras and semiregular variables. These data will provide the input for a forthcoming second paper (Aringer et al. in preparation) that will deal with a comparison of our findings with atmospheric models focusing on the behavior of the SiO lines as in the previous papers by Aringer et al. (1997, 1999b).

## 2. Molecular data

### 2.1. OH

The hydroxyl free radical is a well known contributor of vibration-rotation lines to the spectra of K and M stars. Aringer (2000) finds that OH appears in giant spectra at an effective temperature below approximately  $4200\ \text{K}$ . The OH molecule is well known for the three maser lines in the rotational spectra of AGB stars at  $1612$ ,  $1665$  and

Send offprint requests to: lebzelter@astro.univie.ac.at

\* Operated by the Association of Universities for Research in Astronomy, Inc. under cooperative agreement with the National Science Foundation

1667 MHz, respectively. These lines provide an important tool for deriving accurate center-of-mass velocities of AGB stars (see Habing 1996 for a review). Within our sample of stars OH masers have been detected only in R Cas and R Leo (Benson et al. 1990). The maser lines are much lower energy transitions than any of the OH lines discussed in this paper and are formed in the expanding circumstellar shell.

The 3-4  $\mu\text{m}$  region contains the vibration-rotation fundamental bands of OH. The first overtone vibration-rotation bands are found around 1.5  $\mu\text{m}$ . Due to the low molecular weight of OH, the rotational constant is large and OH does not form band heads in the P branches in the near infrared. The OH lines are out of the  $X^2\Pi$  ground state and exhibit large lambda doubling. Hence the lines appear in quartets in the spectrum. A detailed study of the first overtone OH lines in the mira variable R Leo is described by Hinkle (1978). Line positions derived from Coxon (1980) and Coxon & Foster (1982) are used in the current paper. The line list consists of a group of 17 1-0 and 2-1 P branch lines selected from the total of 46 lines in the 2500 to 2800  $\text{cm}^{-1}$  region. The chosen lines have minimal blending with telluric and other stellar features. The entire set of 46 lines was used to evaluate the measurement process as described below.

## 2.2. SiO

SiO is, after CO and  $\text{H}_2$ , one of the most abundant molecules in the atmospheres of oxygen-rich AGB stars. It is formed in all cooler oxygen rich stars. Model spectra indicate that significant amounts of SiO are formed in stellar atmospheres with effective temperatures of approximately 4000 K or less (Aringer 2000). In addition to being abundant, SiO is a primary constituent of oxygen-rich dust. Since dust is one of the requirements for AGB mass loss (Gail & Sedlmayr 1986), SiO formation is a prerequisite for mass loss.

SiO maser emission is very common among miras (Jewell et al. 1991). Beside sharp maser lines, broad thermal SiO emission in rotational lines has been detected in several AGB stars (see Habing 1996 for a review). Some SiO maser lines involve relatively large J rotational transitions. These lines could be formed near the same region probed by the infrared vibration-rotation SiO lines. Two infrared SiO vibration-rotation transitions have been observed in late-type stars. The fundamental bands are found in the spectrum near 8  $\mu\text{m}$ . The first overtone bands are found near 4  $\mu\text{m}$ . We report here on measurements of lines from the first overtone.

Unlike OH, the SiO line spacing is small. This spacing combined with the transitions occurring in a  $X^1\Sigma$  state results in well defined R-branch band heads. The first high resolution spectra of the SiO first overtone lines in a star were obtained by Beer et al. (1974) who used the spectra to derive Si isotopic abundances in  $\alpha$  Ori. Observing

the band heads at medium spectral resolution, Hinkle et al. (1976) found that long period variables show a strong variability in the intensity of the SiO bands at 4  $\mu\text{m}$ . In miras, around light maximum SiO becomes almost undetectable, strengthening towards light minimum. This result has been confirmed by Rinsland & Wing (1982), who also noted that SiO absorption features are most prominent in stars with the lowest temperatures (i.e. at light minimum in miras). Different explanations for the strange behavior of SiO in AGB variables have been discussed including dissociation, additional absorption (e.g. by  $\text{H}_2\text{O}$ ) or emission of SiO (Rinsland & Wing 1982, Aringer et al. 1999b). The only published high resolution spectra of the first overtone bands of SiO in AGB variables is an atlas of the 4  $\mu\text{m}$  range by Ridgway et al. (1984).

The SiO line list used in this paper is made up of 20 unblended  $^{28}\text{SiO}$  lines in the 2-0 R branch between the 3-1 band head and the 2-0 band head (2-0 R22 to R46) spanning the wavenumber interval 2475 to 2493  $\text{cm}^{-1}$ . The frequencies used are those reported in Hinkle et al. (1995).

## 2.3. HCl

There are no previous detailed investigations of HCl in cool evolved stars. Ridgway et al. (1984) report lines of HCl in the 4  $\mu\text{m}$  spectrum of the S-type mira R And, but they did not find HCl in oxygen- or carbon-rich AGB stars. The HCl vibration-rotation fundamental crosses the 3-4  $\mu\text{m}$  region. The transition is a  $X^1\Sigma$  and since HCl, like OH, is a hydride the rotational constant is large and hence the line spacing is large without prominent band heads. The frequencies of the lines are taken from Le Blanc et al. (1994). Lines of both the  $\text{H}^{35}\text{Cl}$  and  $\text{H}^{37}\text{Cl}$  isotopes were used. This augments the rather spare number of lines present and since the solar system  $^{35}\text{Cl}/^{37}\text{Cl}$  is small (about three) the intensities of the lines from the two isotopes should be similar. The line list includes 20 lines with the least blending selected from the 1-0 and 2-1 bands limited to the wavenumber region between 2500 and 2800  $\text{cm}^{-1}$ .

## 2.4. $\text{H}_2\text{O}$

Water was first observed in the infrared spectra of cool stars in the early 1960s (see Spinrad & Wing 1969). Later in that decade observations showed water bands to be very strong, variable features in mira spectra (Johnson & Mendez 1970). Recently Alvarez et al. (2000) concluded that the detection of deep water bands in stellar spectra is a direct indication of pulsation. Early workers also recognized that despite water's large abundance in cool, oxygen-rich stars, observations of this molecule from the ground are inhibited by water bands in the earth atmosphere. Water must either be observed from space (Aringer et al. 1999a; Matsuura et al. 1999; Truong-Bach et al. 1999; Yamamura et al. 1999) or by using excited

levels which are populated in atmospheres of stars but are not populated in the Earth's atmosphere (Hinkle & Barnes 1979).

In addition to the vibration-rotation infrared spectrum of H<sub>2</sub>O, this molecule has a rich pure rotational spectrum in the microwave and far-infrared. While considerable blockage of this spectrum also occurs as a result of water in the Earth's atmosphere, water maser lines are known in circumstellar envelopes of evolved stars (Menten & Melnick 1989) including three of our program stars, namely R Cas (Colomer et al. 2000), R Leo (Menten & Young 1995), and RX Boo (Colomer et al. 2000).

The spectrum of water in the atmospheres of LPVs originates in two distinct regions of the star's atmosphere: Most of the lines are formed in the circumstellar region closest to the star, while some lines follow the photospheric behavior and therefore originate much deeper in the atmosphere (Hinkle & Barnes 1979; Matsuura et al. 1999). Infrared H<sub>2</sub>O absorption cannot originate far out in the circumstellar envelope as this would not be consistent with the mass loss rates found in these objects. Tsuji et al. (1997) and Tsuji (2000) argue that the non-photospheric water lines indicate the existence of a warm molecular envelope.

In this paper we will discuss high excitation lines of the  $\nu_3$  vibration-rotation band which are present in the 4  $\mu$ m spectrum. The band origin is at 3756 cm<sup>-1</sup>. The line list consists of 102 high excitation  $\nu_3$  lines between 2500 and 2800 cm<sup>-1</sup>. The frequencies are from Zobov et al. (2000). The line list used for this paper involves moderately high rotational (J) quantum numbers between 12 and 24 and should not include lines formed in the inner circumstellar region. However, we note that like the OH and HCl transitions, the  $\nu_3$  transition is a fundamental vibrational transition. Fundamental transitions are the most likely to be detected in cool conditions and are also the preferred routes for radiation resulting from recombination.

### 3. Observations

The spectra were obtained by one of us (K.H.H.) with the Fourier Transform Spectrometer (FTS) operated at the Mayall 4m telescope at Kitt Peak National Observatory. A description of the instrument can be found in Hall et al. (1979). The FTS is no longer available for use, having been closed in the mid-1990's. The spectra are an inhomogeneous set, having been observed for several projects. However, all cover the 2400 to 2800 cm<sup>-1</sup> region required by the line lists. The resolution achieved is about R=100000 except for very few observations at a somewhat lower resolution but none below 50000. The observations were obtained mainly between 1984 and 1986 with a few additional spectra observed earlier. Three spectra of  $\chi$  Cyg were observed in 1994 and 1995, shortly before the FTS on Kitt Peak was closed. All data have been reduced as described in Hinkle et al. (1982).

**Table 1.** Observing log for the miras. The period in column 3 is taken from the GCVS.

GCVS name	Var. type	Period	JD 2440000+	Visual phase	S/N
R Cas	Mira	430	5986	0.54	53.7
			6018	0.61	106.7
			6108	0.82	27.7
			6160	0.94	87.9
			6192	0.01	47.7
			6223	0.09	52.1
			6243	0.13	35.1
			6312	0.29	92.6
			6454	0.62	44.0
			6510	0.75	50.2
			6570	0.89	58.4
o Cet	Mira	332	3437	0.89	243.4
			4775	0.81	108.6
			5986	0.45	63.2 <sup>1</sup>
			6018	0.55	93.4
			6095	0.78	... <sup>2</sup>
			6108	0.82	57.6
$\chi$ Cyg	Mira	408	6312	0.43	66.6
			3437	0.17	135.9
			5986	0.35	53.8
			6018	0.43	88.0
			6108	0.65	75.0
			6160	0.77	86.3
			6192	0.85	85.8
			6223	0.93	65.2
			6243	0.98	36.0
			6312	0.15	71.4
			6346	0.23	59.4
			6427	0.43	22.0
			6454	0.50	50.6
			6510	0.63	64.4
R Leo	Mira	310	6570	0.78	65.4
			9323	0.62	89.4
			9363	0.71	93.7
			9450	0.93	88.0
			9612	0.30	120.1
			9798	0.75	66.3
			4650	0.60	329.2
			5986	0.76	70.3
			6164	0.31	54.6
			6427	0.15	24.4
			6511	0.41	74.6

<sup>1</sup> two spectra

<sup>2</sup> no reverse scan

For four miras the data set includes time series of 4  $\mu$ m spectra, allowing the stellar pulsation to be monitored. There are also single epoch observations of a number of semiregular variables. Together with some fundamental parameters from the General Catalogue of Variable Stars (GCVS, Kholopov et al. 1985–88), the observational details are given in Tables 1 and 2. Phases are calculated from the closest light maxima provided by the AAVSO (Mattei 1984–95). As can be seen from Table 1 for three of the four miras (R Cas, o Cet and  $\chi$  Cyg) ob-

**Table 2.** Observing log for the semiregular variables. The period in column 3 is taken from the GCVS. Phases are rough estimates from AAVSO light curves.

GCVS name	Var. type	Period	JD 2440000+	Visual phase	S/N
RZ Ari	SRb	30	7071	–	
RX Boo	SRb	340	6986	0.0:	
W Cyg	SRb	131	6160	0.4:	42.8
RU Cyg	SRa	233	6160	0.2:	16.9
g Her	SRb	89	6986	0.9:	... <sup>1</sup>
R Lyr	SRb	46	6986	–	
SW Vir	SRb	150	6986	–	

<sup>1</sup> no reverse scan

servations from different light cycles but at similar phases exist. This can be used to investigate the cycle to cycle behavior of these stars (see below). The dust enshrouded object IRC+10216, which is a featureless, bright continuum source at 4  $\mu\text{m}$ , was also observed. The IRC+10216 spectrum allows easy identification of telluric lines.

Seven stars of our sample (all miras, RU Cyg, W Cyg, g Her) have previously been investigated using 1.6  $\mu\text{m}$  spectra (Hinkle et al. 1982, 1984, 1997 and Lebzelter 1999). These papers also give a summary of the fundamental properties for these stars from the literature. Three miras of our sample are ‘typical’ representatives for oxygen rich disk miras with respect to period, amplitude, spectral type and mass loss. Since they are among the brightest miras in the sky, these objects are very well studied. The fourth mira is  $\chi$  Cyg, a S-type star, the pulsational behavior of which has been studied in detail by Hinkle et al. (1982) and Wallerstein (1985).

The spectra are very blended and it is typically not possible to find ‘clean’ individual line profiles. Hence we have worked from average line profiles calculated from all lines of the list. Velocities have been determined from the deepest point in the average profile of the lines for each of the four molecules investigated. In many cases this velocity summarizes a blend so, in addition, the average profiles themselves are discussed below. The line lists typical contain about 20 lines for each molecule of similar intensity and excitation. For water, many more lines were available and as can be seen in the average profiles the ‘noise’ was significantly reduced.

The average profile is modified by blending lines around each of the individual line positions. Given the high level of blending of some spectra it is remarkable that a reasonable average profile emerges. In this light it is critical that the average line profiles not be over interpreted. We feel that the general features, especially those seen in time series and in the profiles of other molecules, are real. However, detailed features seen only in one profile could be artifacts of the averaging process. In the case of OH we performed a test where average profiles were made up from two independent line lists of 23 lines each.

There was remarkable agreement between the two profiles, indicating that essentially all the features are real.

The velocity of telluric lines was measured to check on the zero point of the velocity scale. This correction is typically done in FTS spectra because the reference and stellar beams can have non-parallel paths. In each of the 4  $\mu\text{m}$  spectra we found the telluric velocities to be distributed around zero with a full width at half maximum of this distribution of about 0.1 km s<sup>−1</sup>. At longer wavelength alignment errors become less significant and this seems confirmed by this data set. Applying the small, apparently random telluric correction would increase the uncertainties and hence we have not done so. In any case the correction is less than or on the order of  $\pm 0.2$  km s<sup>−1</sup> in the measured velocities. Further details on 4m FTS data and FTS data reduction can be found in Hinkle et al. (1984, 1995).

#### 4. Mira Results

Time series of averaged SiO, H<sub>2</sub>O, HCl and OH lines of RCas are plotted in Figs. 1 and 2, respectively. Typical line profiles from the other three miras can be found in Figs. 3 to 6. No continuum is marked in the figures as the true continuum is at a much higher level due to the almost continuous absorption by weak H<sub>2</sub>O lines (and similar molecules) in this spectral region. The line profiles shown are averaged line profiles so that the range to both sides of the line can be used to define some kind of pseudo continuum. In Figs. 1 to 4 spectra have been normalized to this pseudo continuum. The center-of-mass velocity, for all objects from radio observations of thermal CO, is marked in the figures (references on the center-of-mass velocity as well as previously measured infrared and visual velocities can be found in Hinkle et al. 1982, 1984, 1997). Lines could be detected at all phases but vary considerably in shape and strength. A quick comparison of similar phases shows sometimes large variation in the line profiles between the same phase in different light cycles for the same star (e.g. compare the spectra obtained at phase 0.61 and 0.62 in Fig. 1). In the 4  $\mu\text{m}$  region RCas is an extreme example of cycle-to-cycle variations. The other miras of our sample show some differences between line profiles obtained from different light cycles at similar phases but these differences are typically not as large as in RCas. Note that observations obtained at similar phase but several years apart can also have very similar profiles (e.g. Fig. 5). This is suggestive of a strong aperiodicity as well as a periodic variation in the spectra. This is a common comment made about visual spectra and some features (e.g. low excitation 2-0 CO lines) in 2  $\mu\text{m}$  spectra but is not seen in the highly periodic behavior of the great majority of lines in the 1.6-2.5  $\mu\text{m}$  region (e.g. Hinkle et al. 1982).

Emission components are clearly visible in several observations. This suggests a filling of the absorption with

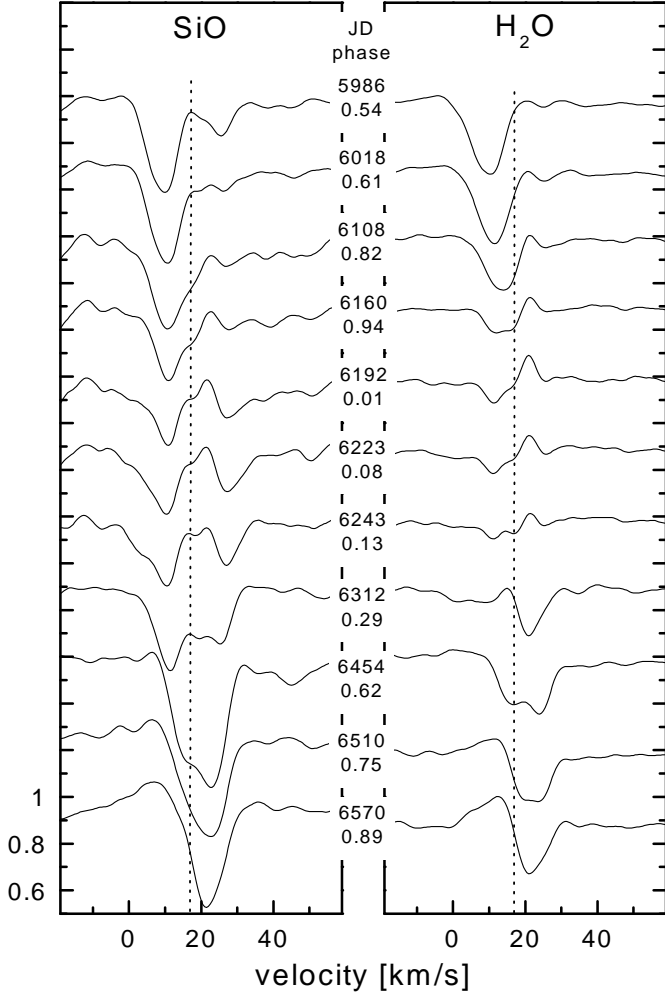


**Fig. 1.** Averaged SiO 2-0 (left) and H<sub>2</sub>O  $\nu_3$  (right) line profiles of R Cas. Date of observation and according phase are given in the plot. The dotted line marks the center-of-mass velocity.

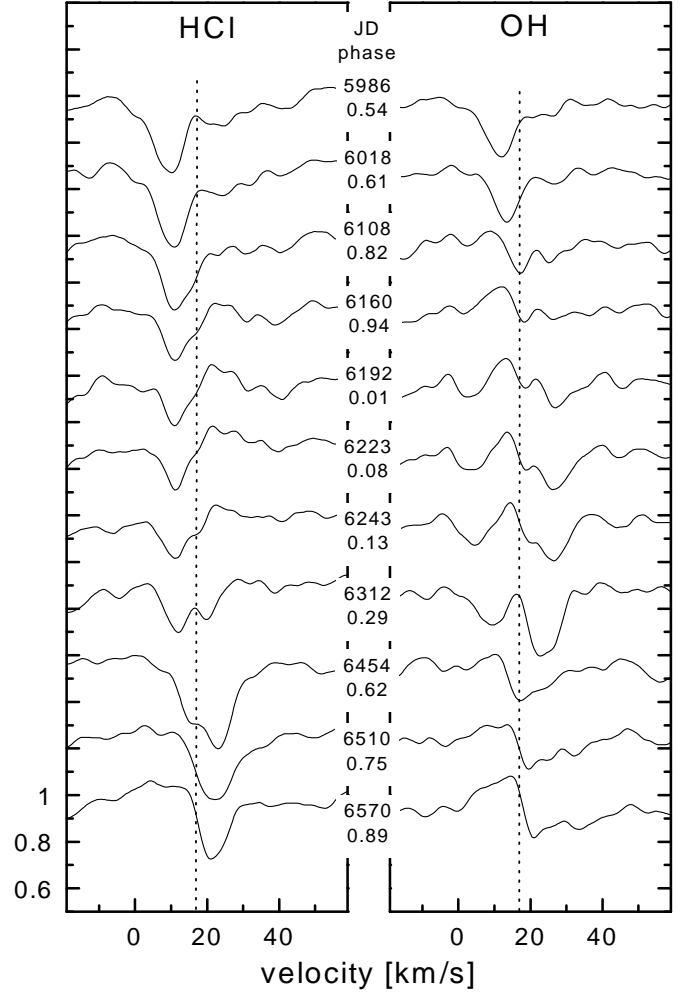


**Fig. 2.** Averaged HCl fundamental 1-0, 2-1 (left) and OH fundamental 1-0, 2-1 (right) line profiles of R Cas. Date of observation and according phase are given in the plot. The dotted line marks the center-of-mass velocity.

emission as an explanation for the weakening of the SiO lines observed in low resolution spectra as proposed by Aringer et al. (1999b). Multiple absorption components with varying strength are an obvious characteristic of the investigated lines in most of the spectra. Unresolved multiple emission components also appear.

For a given observation the four molecules investigated, OH, H<sub>2</sub>O, SiO and HCl, differ quite strongly in the shape of their line profiles. OH, as seen in the R Cas spectra, can show an emission line while the other three molecules show an absorption line. Among the studied oxygen rich miras differences of this type are largest for R Cas and smallest for R Leo. In  $\chi$  Cyg OH and H<sub>2</sub>O behave much more similarly than in the other stars of our sample as illustrated in Fig. 3. Furthermore, the four molecules also differ in their variability. In the following we will now discuss the line profile variations for each molecule separately. We will offer an interpretation of the

complex line structures seen keeping in mind the limitations of doing this without detailed model calculations.

If not explicitly stated velocities and velocity shifts mentioned in the following are relative to the center-of-mass velocity of the star. The convention is used with negative velocity indicating outflow of material. The line profile figures have heliocentric velocity for the abscissa.

#### 4.1. OH

Fig. 7 gives the resulting velocities derived from OH lines for R Cas and  $\chi$  Cyg plotted against time. Time is selected for the abscissa rather than phase since the variability does not always follow the photometric period. Velocities were determined only for those absorption components of the line which could be clearly identified and attributed to the line investigated. As can be seen in Figs. 1 and 2, other weak absorption components can exist in the line

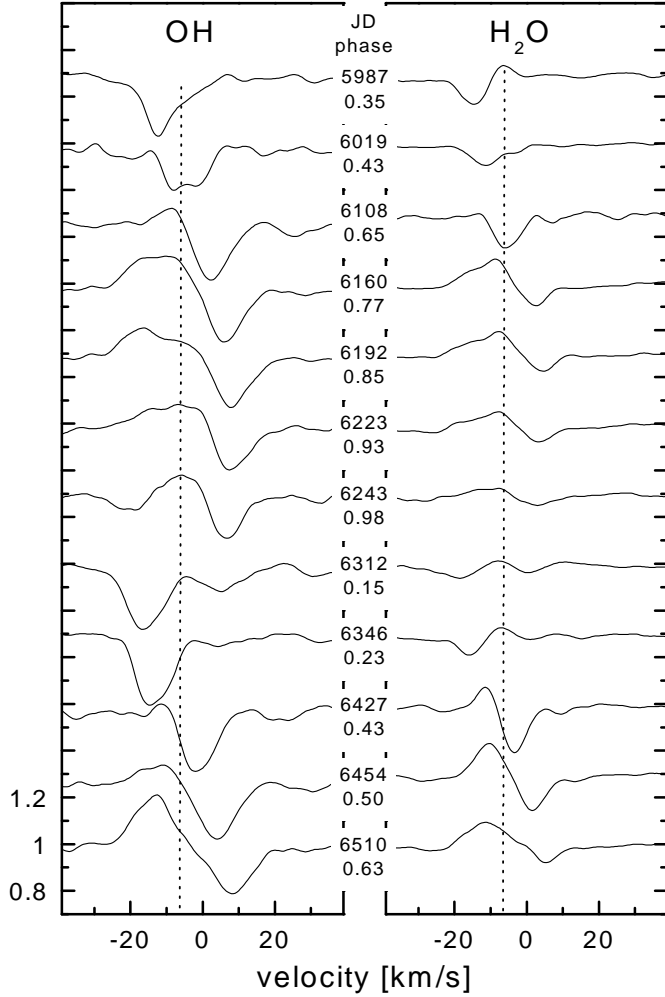


**Fig. 3.** Averaged OH fundamental (1-0, 2-1) (left) and H<sub>2</sub>O  $\nu_3$  (right) line profiles of  $\chi$  Cyg. Date of observation and according phase are given in the plot. The dotted line marks the center-of-mass velocity.

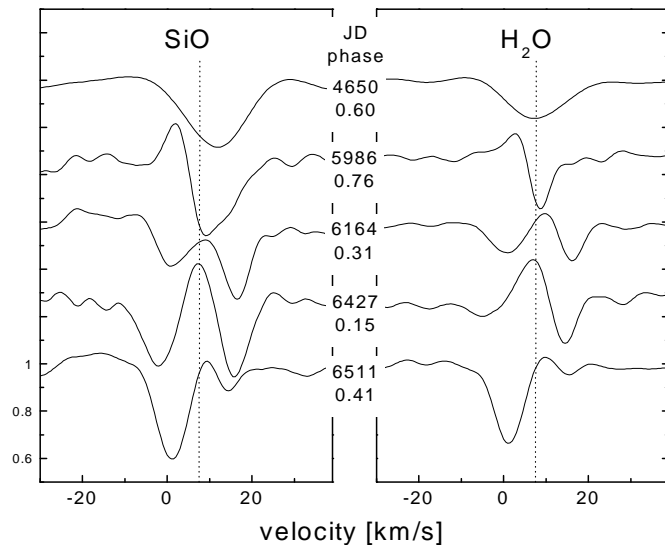


**Fig. 4.** SiO & H<sub>2</sub>O line profiles of R Leo. Same as Figure 1.

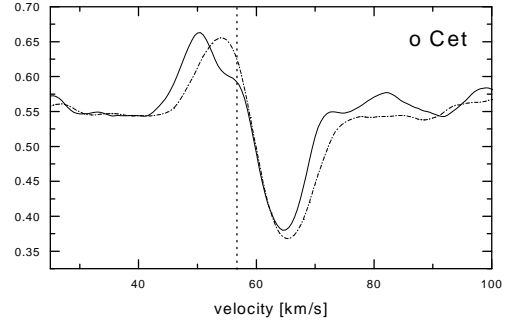


**Fig. 5.** Averaged SiO line profiles from two observations of o Cet at similar phase but widely separated in time. The solid line is the profile from Feb 11 1985 ( $\Phi = 0.82$ ), while the dash-dotted line marks the profile at Oct 21 1977 ( $\Phi = 0.89$ ). The dotted vertical line indicates the center-of-mass velocity.

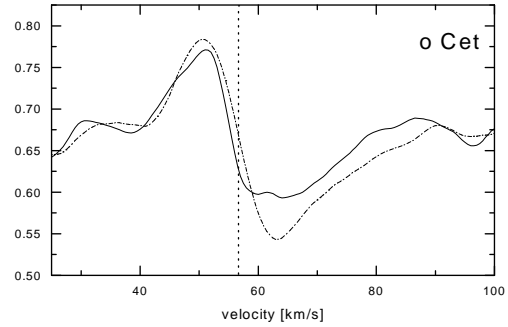


**Fig. 6.** Same as Figure 5 for OH.

profiles. Obviously for complex line profiles such as these the velocities are subject to interpretation. For instance, doubled absorption can result from an emission line filling the center of a broad absorption line. We base the results extracted from the averaged line profiles on similarities found for CO lines of different excitation published before (e.g. Hinkle et al. 1982). For  $\chi$  Cyg only the measurements between 1984 and 1986 have been plotted to allow for the same time interval as R Cas.

For both stars we see a velocity curve resembling the velocity curves found for CO first overtone high excitation lines in the 2.3  $\mu$ m region (see e.g. Hinkle et al. 1982). However, a closer inspection reveals significant differences between the two stars and relative to the CO velocity curve. For R Cas we have a phase of line tripling between JD 2446190 and JD 2446300 (see the individual line profiles in Fig. 2). The first part of the velocity curve shows a layer at rather constant infall velocity and a variable component changing from outflow to infall. During this time of infall, absorption is becoming visible at an outflow velocity again. Surprisingly, the temporal separation between observations of similar velocity is shorter than the pulsation period of 430 days, in the one cycle examined it is  $\sim 300$  to 350 days. However, this behavior is clearly not related to the general pulsation of the star since the

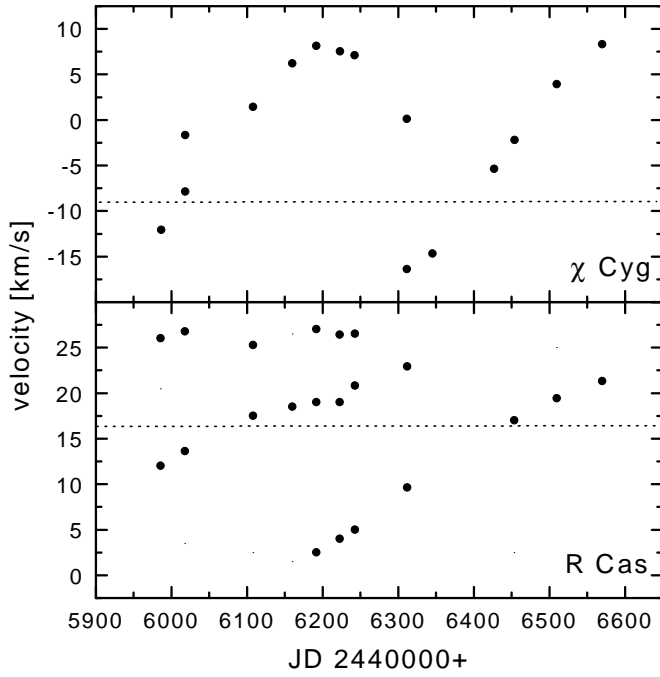


**Fig. 7.** Velocities measured from absorption components of OH lines in  $\chi$  Cyg (upper panel) and R Cas (lower panel). The dotted line indicates the center-of-mass velocity.

AAVSO light curve of R Cas at the time of the infrared spectroscopy shows a cycle length of the typical 430 day photometric period. The only notable deviation from the normal light cycle is a very bright maximum preceding the time these spectra were observed. The first light maximum we monitored has been a slightly weaker than usual. The absorption at constant infall velocity is not visible in the second half of the studied time interval and there is also no indication of a further line doubling at the end of the second cycle around JD 2446600.

In  $\chi$  Cyg OH shows velocity changes with the period of the photometric variations, i.e. observations of similar velocity are separated by roughly one period of the star. Between the two cycles we have one observation with absorption line doubling. We also found line doubling on JD 2446749, but with a much smaller velocity difference. In addition, we note that the averaged line profiles of  $\chi$  Cyg indicate further phases of line doubling, but in these cases the second component is very weak not allowing an accurate velocity determination.

Beside the absorption components OH emission is visible at several phases and can be quite strong. In the R Cas spectra an OH emission component can be detected at all phases, but in several spectra it is not obvious since the emission peak is embedded in the absorption profile resulting in a weaker emission line that does not exceed the level of the continuum. The emission component starts at the blue end of the line at a velocity relative to the

center of mass of roughly  $-14.5 \text{ km s}^{-1}$  (i.e.  $+2 \text{ km s}^{-1}$  heliocentric) and moves redwards. Around JD 2446312 the emission component reaches the center-of-mass velocity. Four months later a new emission line is visible at the blue edge of the line again. It is not clear whether the first emission line is still visible – now at an infall velocity – on JD 2446510. On the other hand, the second emission line can already be visible when the first one reaches the center-of-mass velocity. Unfortunately, the coverage of the variability is not very good during this phase.

We conclude that the line profile of OH in R Cas is produced by the combination of one or two absorption lines, one outflow and one infall component, which means the occurrence of line doubling at some but not all phases. An emission line is running from the blue to the red end of the red shifted line. The absorption lines vary in strength and slightly in velocity during the cycle and from cycle-to-cycle. The emission component can become quite strong, so that it becomes visible above the continuum level. A weak emission component with an infall velocity seems to be present in several spectra. The line profiles of the other three miras of our sample can be interpreted in the same way. In this way we can also explain the unexpected line doubling in  $\chi$  Cyg on JD 2446006 as the passage of an emission component through the line core.

#### 4.2. SiO & HCl

Representative line profiles for SiO and HCl in the R Cas, oCet and R Leo spectra are illustrated in Figs. 1, 5 and 4, respectively. Strong emission components of SiO and HCl are seen in several spectra of R Leo and oCet, and also in the spectra of  $\chi$  Cyg. In R Cas emission components are clearly weaker.

The line profiles of these two molecules show similar and complex behavior with both emission and absorption. As examples the velocity curves of R Cas and  $\chi$  Cyg are discussed (Fig. 8). One absorption component of the SiO and HCl lines in  $\chi$  Cyg at a velocity of about  $+10 \text{ km s}^{-1}$  relative to the systemic velocity of the star (about  $+0.5 \text{ km s}^{-1}$  heliocentric) is visible in all SiO and HCl spectra of our data set, including spectra obtained outside the time range plotted in Fig. 8. In addition there is in  $\chi$  Cyg a second absorption component at several phases shifting its velocity towards that of the first component. The period observed in these data is about 320 days, conspicuously less than the photometric period. Note that the velocity curves of the two cycles of  $\chi$  Cyg observed are not parallel. We will discuss this difference in more detail in the next section.

R Cas has quite different velocity variations compared to the other miras studied. From Figure 1 we see that from JD 2445987 to JD 2446192 the outflow component of the SiO lines is dominant in the spectrum, while from JD 2446454 to JD 2446570 the infall component is clearly stronger. Yet the absorption components have similar



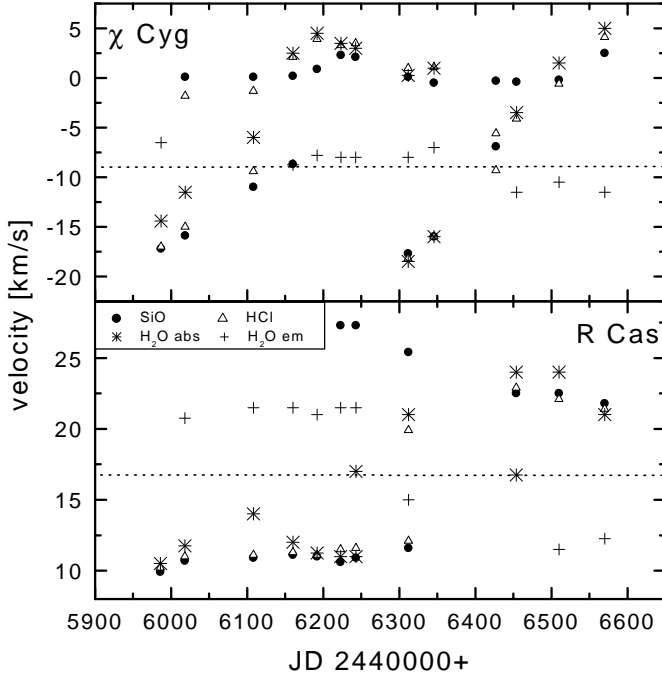


**Fig. 8.** Heliocentric velocities measured from absorption components of SiO (filled circles), HCl (open triangles), water absorption (stars) and emission (crosses) lines in  $\chi$  Cyg (upper panel) and R Cas (lower panel). The dotted line indicates the center-of-mass velocity.

depths at similar phases. In the spectra obtained in 1986 (JD 2446430 through JD 2446800) the outflow component may be filled by an emission line which is becoming visible in the JD 2446570 spectrum.

A strong emission component is clearly visible in several spectra of R Leo (see Fig. 4), o Cet and  $\chi$  Cyg (Fig. 3). The R Leo data set is an example of spectra where the line profiles can be interpreted as a combination of an absorption line and an emission line, with the absorption and emission having different phase dependent velocity behavior. On the other hand, in R Cas an additional weak emission component at the systemic velocity is seen as an obvious asymmetry in the absorption line. In the R Cas spectra near maximum light, and especially the spectrum of JD 2446192, the strong absorption component of SiO and HCl matches the velocity of the strong (for R Cas) OH emission line.

As the variability cycle of the 4  $\mu$ m molecular features does not always follow the photometric period it is very difficult to compare the line profiles of different miras at similar visual phases directly. However, basic characteristics, namely outflow and infall components, intensity variations, and the occurrence of emission at some phases, are found in all miras of our sample. The similarity between the SiO line profiles and the HCl line profiles is a common feature of all stars. In general, line profile and variability is

similar in R Leo, o Cet and  $\chi$  Cyg. R Cas shows a different, more complex behavior.

#### 4.3. $H_2O$

The  $H_2O$  line profiles do not follow the variations of either the OH or the SiO and HCl line profiles. This is illustrated by comparison of  $H_2O$  line profiles with those of other molecules in Figs. 1, 3 and 4. The dissimilarity of profiles indicates that, at least at some phases, the  $H_2O$  lines probe a very different atmospheric zone than the lines of the other molecules seen in the 4  $\mu$ m spectra. In addition, we note that the  $H_2O$  lines in  $\chi$  Cyg are weak in agreement with the S-type spectral class of this star (Fig. 3). Emission components, which can be seen in other molecular lines, are even more prominent in  $H_2O$  line profiles.

Velocities derived from absorption and emission components of the  $H_2O$  line profiles of R Cas and  $\chi$  Cyg are plotted in Fig. 8 together with the results from SiO and HCl. The  $\chi$  Cyg  $H_2O$  absorption lines show a velocity variation similar to the other three molecules monitored in this stars spectrum. The velocity curve is slightly offset from the SiO and HCl variations, mimicing the velocities of the OH and CO lines but with smaller amplitude. In the one case where the CO and  $H_2O$  velocity significantly differ the cause is probably a blend of the emission and absorption line profiles. The emission component stays almost constant in velocity close to the center of mass velocity throughout the entire light cycle.

R Cas velocities (lower panel of Fig. 8) again have quite different phase dependent behavior than those of  $\chi$  Cyg. One  $H_2O$  absorption component shows a S-shaped discontinuous velocity curve apparently spanning the entire time of observations, i.e. at least two light cycles! Additional absorption components resemble the velocity behavior of SiO and HCl around JD 2446200. The emission component seen in  $\chi$  Cyg close to the center-of-mass velocity is not found. Emission is instead seen at an infall velocity first and switches to an outflow velocity shortly after the visual light maximum at JD 2446200. The overall behavior of the 4  $\mu$ m spectral lines in R Cas is outstanding and will be discussed below.

### 5. Mira Dynamics

Monitoring of the velocity variations of spectral lines provides a powerful tool for studying the physical characteristics and dynamics of the stellar atmosphere. In this section we summarize observed velocity variations for the two miras with the most complete time series,  $\chi$  Cyg and R Cas. On this basis we discuss the dynamics of the outer layers of an AGB star's atmosphere.

There are two basic features of the 4  $\mu$ m spectra that need to be explained by any model: the occurrence of an emission component and the deviation of the variability from the photometric period. However, we stress that even

a qualitative description of these phenomena has to be limited to some basic statements due to the complex, not fully understood structure of AGB atmospheres. It can be difficult to discern observationally the movement of a layer and a change in the optical depth since they can produce interfering results. The emission component may have its origin in the atmospheric dynamics or in a geometrical effect. We will discuss the absorption components first and come back to the emission lines at the end of this section.

### 5.1. $\chi$ Cyg

The  $\chi$  Cyg spectra described above provide the most extensive and well sampled time series of  $4\mu\text{m}$  spectra of any star in our sample.  $\chi$  Cyg also has good time series spectra in the H-band and K-band which cover the first and second overtone lines of CO. We will summarize the velocity data for this star as an example of the overall relation between the dynamics of atmospheric layers as probed by different molecular features in the infrared.

The second overtone CO lines at  $1.6\mu\text{m}$  are thought to provide information about the kinematics deep inside the atmosphere, i.e. close to the pulsation driving zone (Hinkle 1978). The corresponding velocity curve is S-shaped with line doubling occurring around maximum in all miras. The line doubling is seen only in miras, not in the lower amplitude semiregular variables. In miras the center-of-mass velocity is crossed by the velocity curve typically around phase 0.4. At that phase no line doubling occurs in these stars. A similar behavior is shown by the high excitation first overtone CO lines found in the  $2.3\mu\text{m}$  region. For  $\chi$  Cyg an extensive time series of these lines has been published already (Hinkle et al. 1982). For the present investigation a new set of  $1.6\mu\text{m}$  spectra was taken in order to compare the  $4\mu\text{m}$  results with *simultaneous* data from CO lines. The  $1.6\mu\text{m}$  spectra were obtained with the same instrumental setup as the earlier measurements published in Hinkle et al. (1982).

Figure 9 shows the velocities of the different molecular species versus time for the mira  $\chi$  Cyg. Visual phase relative to the first maximum observed (phase 0.0) has been added as label to the top axis. As demonstrated previously (Hinkle et al. 1982) the CO lines vary with the photometric period. Line doubling is visible around maximum. There is no difference between the CO velocity curve presented here and those obtained earlier by Hinkle et al. (1982). The  $4\mu\text{m}$  OH lines in  $\chi$  Cyg follow the behavior of the CO lines. In general the  $\text{H}_2\text{O}$  absorption line velocities for  $\chi$  Cyg follow the CO velocity curve.

The velocity curve defined by the SiO lines is clearly different from the CO line curve. As mentioned above SiO has a more or less constant velocity component at an infall velocity of about  $10\text{ km s}^{-1}$ . There is no feature in the CO or OH profiles that could be correlated with the first absorption component of SiO at constant velocity. A smaller

velocity amplitude is seen in SiO (and also in HCl, see Fig. 8) lines.

SiO also has a second absorption component that shows strong variability in velocity. But this variation is not always quite with the stellar pulsation. During the first cycle observed for  $\chi$  Cyg the line forming region of SiO decelerates less than the CO and OH line forming region, assuming that the lines of a certain species originate in the same layer at all phases. During this cycle the braking effect is smaller for this layer. In the second light cycle SiO has a velocity component that follows the CO velocity curve.

A possible explanation is that mass loss is not continuous, with material ejected in shells but not during every light cycle (e.g. Winters et al. 2000). Several observations in the radio range and of post-AGB objects support this description of the mass loss. If so, material would be aggregated at some distance from the star before it is ejected. A mass shell reaching this distance during its pulsation will be then confronted with more or less material, i.e. with an environment with varying density from cycle-to-cycle. If there is less material, the layer or a moving wave can go faster and further away from the star and in this way again would feed the mass loss. The problem with the time between phases of similar velocity being shorter than the photometric period can in that way be explained. The layers traced by the SiO (and also by HCl) are not varying on a shorter time scale but with a different acceleration during some cycles. After several cycles we can again have similar line profiles as observed in o Cet and  $\chi$  Cyg.

### 5.2. R Cas

The mira R Cas shows a behavior remarkably different from  $\chi$  Cyg, especially corresponding the velocities of OH and SiO lines. No simultaneous CO observations are available for this star. Comparison with older data (Hinkle et al. 1984) shows that the velocity curve derived from the OH lines has a flatter slope than the CO velocity curve. The maximum expansion velocity observed in OH is smaller than the one observed in the CO lines.

The  $\text{H}_2\text{O}$  lines in R Cas are the only ones found that indicate the presence of (periodic) variations in the outer layers of the atmosphere with a time scale longer than the period indicated by the visual light change. In Fig. 10 we show that the different  $\text{H}_2\text{O}$  absorption components can be grouped to two nicely shaped velocity curves by two hand drawn fits through the data points. The curves are numbered '1' and '2', respectively. Curve '1' as noted above covers a time scale exceeding the photometric period, while the variation represented by curve '2' happens on a time scale similar to the main period. Curve '2' also shows the same relation between velocity and light change found e.g. for high excitation CO lines, i.e. minimum velocity at light maximum. However, no line doubling of the

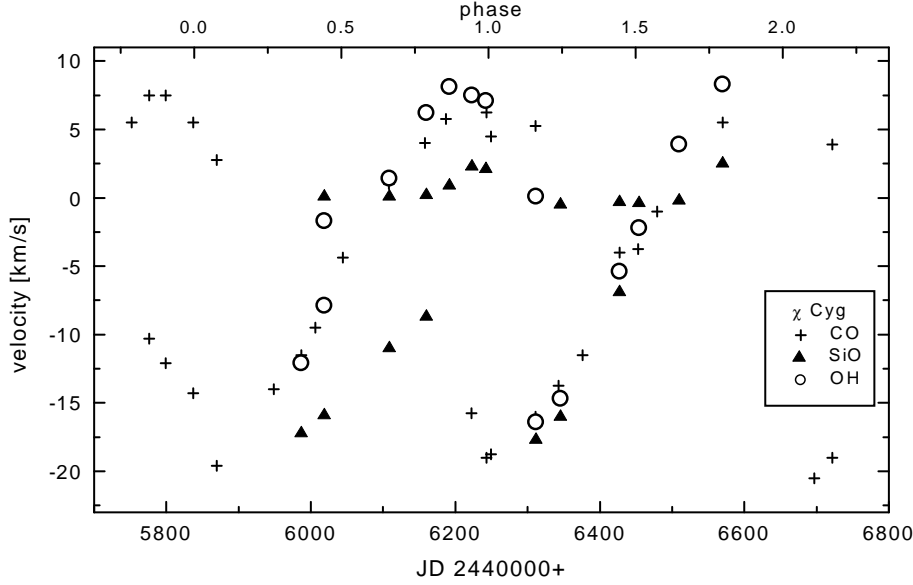


**Fig. 9.** Velocities of different molecular lines versus time and visual phase for  $\chi$  Cyg. The visual phase given at the top axis is relative to the visual light maximum at JD 2445838. Crosses mark velocities from CO lines, triangles SiO velocities and open circles OH velocities, respectively.

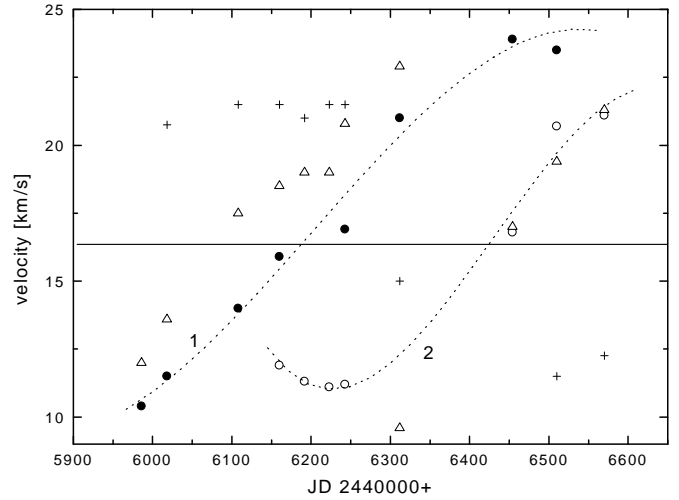
same type as in the CO lines is observed for curve '2', as any second absorption component fits on curve '1'.

Fig. 10 shows the velocities of the OH lines as well. It can be seen that they form a velocity curve of similar shape as the H<sub>2</sub>O lines but with an offset. The first part of the OH velocity curve shows also the same velocity *range* as the H<sub>2</sub>O lines while the second velocity curve found from the OH lines has a larger range in velocity. This may indicate that our time series does not cover the whole length of this long period change, so that the time scale may be even larger than two times the main period.

The line doubling of the H<sub>2</sub>O lines suggests that during some phases we see line forming layers at two completely different locations in the stellar atmosphere. The similarity in the behavior of curve '2' and the high excitation CO lines implies that curve '2' represents a layer close to the pulsation driving zone. It is interesting to note that we did not find any absorption components that would mark this layer around JD2446000.

Based on these results we propose the following scenario occurring in R Cas: Around JD2445800, i.e. at the light maximum preceding our time series, a cycle of velocity variations started that lasted much longer than a typical cycle. A similar model as for the SiO line forming layer in  $\chi$  Cyg may therefore be assumed, i.e. that the variation marked as curve '1' in Fig. 10 lasted longer than one cycle as material may have been moved further away from the star and needed a longer time to return to its original position.

Note that our data do not give any indication whether this behavior is occurring with some periodicity or not. The CO lines, observed at a different time, did not show such strange behavior. In this context it is interesting to note that a very bright maximum is preceding this phase of strange velocity behavior. Such bright maxima occur from time to time with no obvious regularity in R Cas (Mattei



**Fig. 10.** H<sub>2</sub>O and OH velocities of R Cas versus time. Filled and open circles mark the two H<sub>2</sub>O absorption components, crosses indicate the velocities of water emission lines, and open triangles denote OH absorption lines. Two velocity curves, marked '1' and '2', have been drawn through the H<sub>2</sub>O data points. The horizontal line indicates the center of mass velocity. See text for more details.

2000). It seems quite probable that these two phenomena are related to each other. At the next light maximum again a velocity curve starts, this time its period is following the photometric changes. Therefore, only in some cycles such strange line profiles may occur.

However, as the behavior of the SiO lines in R Cas shows, this scenario cannot explain the dynamics of the outer atmosphere completely. The SiO lines obviously vary on a time scale longer than the photometric period, but from our data there is no indication for any periodic variation.

### 5.3. Emission lines

Emission can in principle be produced by a temperature inversion, as it would be provided by a shock front or a hot chromospheric layer, or by a geometric effect in an extended spherical object (e.g. Hinkle et al. 2000). Both mechanisms are possible in miras. The occurrence of shock fronts is well known not only from optical spectra but also from the velocity curves derived from second overtone CO lines in the near infrared (e.g. Hinkle et al. 1982). In the optical range emission of hydrogen and several metal lines is triggered by the passage of shock fronts. Chromospheric layers have been proposed from model calculations by Willson & Bowen (1986), but no final observational proof has been given for their existence in oxygen rich AGB stars. Finally, atmospheres of pulsating AGB stars are definitely widely extended and can show a shell like structure in the outer parts (e.g. Höfner 1999).

We note that the emission component of some molecules changes velocity during the time series but other emission components have a near constant velocity. This suggests two separate places for the emission. In RCas we observe an emission component in the OH lines changing from a high outflow velocity to the center-of-mass velocity. If we attribute the emission to a certain moving layer, we would see a braking of the movement until it comes to a stop relative to the center of the star. Such a behavior of the emission has also been seen in emission lines of the Balmer series in miras (e.g. Merrill 1946). However, the emission seen in the H<sub>2</sub>O lines, most notably in  $\chi$  Cyg, is constant in velocity. We propose that this emission is produced in the outer layers of the extended atmosphere. Tsuji (2000) makes similar arguments for emission seen from water in the inner circumstellar shell. The extended atmosphere may also explain emission seen in molecules other than H<sub>2</sub>O in SRV's where there is no indication for a shock front from second overtone CO lines or hydrogen lines (see below).

## 6. SRVs

Semiregular variables are generally believed to have a lower pulsation amplitude than the miras and as a result SRV spectra are expected to be less affected by dynamic phenomena. To study the influence of stellar dynamics on the 4  $\mu$ m spectra of SRVs, we examine in this section representative SR spectra from different period and amplitude regimes. Short period and low amplitude SRVs typically have small mass loss rates and are therefore difficult to detect in thermal radio CO lines (e.g. Kerschbaum & Olofsson 1999). As a result the most reliable information on the center-of-mass velocity for long period variables is not available for these stars. The discussion of velocities relative to the center of mass is therefore limited to the subset of stars where an accurate systemic velocity has been measured.

The SRV observations reported here cover only a single epoch. Due to the lack of reliable photometric data a rough determination of the actual visual phase of the variables at the time of the observation was possible only for three SRVs of our sample. As a consequence we will focus on W Cyg and RU Cyg, for which both velocity and phase determination are quite reliable.

Figs. 11 and 12 show the SiO and OH line profile of the semiregular variables W Cyg and RU Cyg, respectively. The SiO lines in W Cyg show an absorption component on each side of the systemic velocity with the outflow component dominating. Outflow occurs with a velocity of 6 km s<sup>-1</sup>. In contrast the second overtone CO lines show only outflow velocities over the whole light cycle (Hinkle et al. 1997). One of the CO second overtone spectra has been obtained only 2 days before the 4  $\mu$ m observation and gives a heliocentric velocity of -20.0 km s<sup>-1</sup>, i.e. an outflow velocity of about 6 km s<sup>-1</sup> the same as found for the SiO lines. Compared with miras at similar phases (e.g. R Leo, line profile at the bottom of Fig. 4) the SiO lines in W Cyg are weaker. It should be remarked that the SiO lines in W Cyg are the weakest among all the SR spectra in our sample. Comparison with miras is of course difficult due to nonperiodicities. The average OH line profile of W Cyg (bottom panel of Fig. 11) is broad and slightly asymmetric towards the outflow part. As for miras, one possibility is that the doubling of the absorption is produced by an emission component filling in the absorption line, although no indication for a shock front is given in the second overtone CO line velocity curve for W Cyg. However, the emission is strongly supported by the H<sub>2</sub>O profile which shows emission above the continuum with weak absorption on each side. The emission is at -20 km s<sup>-1</sup> heliocentric.

The SiO and OH profiles in RU Cyg are quite different from those of W Cyg. A double structure is visible in the OH lines but not in the SiO lines. The spectrum indicates only outflow of matter. As for W Cyg a spectrum with second overtone lines of CO has been obtained almost simultaneously (Hinkle et al. 1997). The CO lines indicate an outflow, too, with a similar velocity. The profile could of course result from an emission/absorption blend. The  $\nu_3$  lines of water can not be detected in RU Cyg.

The other five SRVs show slightly asymmetric SiO lines with the positive velocity side steeper than the negative velocity side. None of these objects shows any indication of line doubling or emission components in the line core. SiO lines are more narrow in g Her, R Lyr and RZ Ari, i.e. in the stars with periods below 100 days, than in the other SRVs. The OH lines look similar to the SiO lines in these three SRVs. For g Her a reliable systemic velocity is available (Kerschbaum & Olofsson 1999). Neither the SiO lines nor the OH lines show a significant shift relative to this systemic velocity. HCl lines have been detected in all SRVs except for W Cyg. They are much weaker in these stars than in miras.

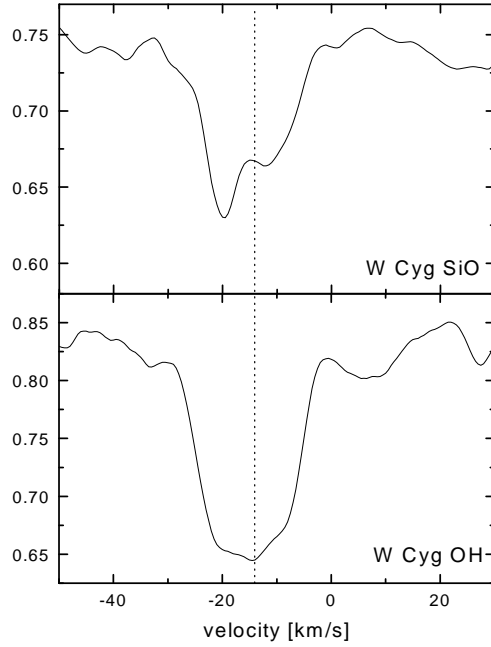


**Fig. 11.** SiO (upper panel) and OH (lower panel) line profiles of W Cyg. The dotted line marks the systemic velocity.

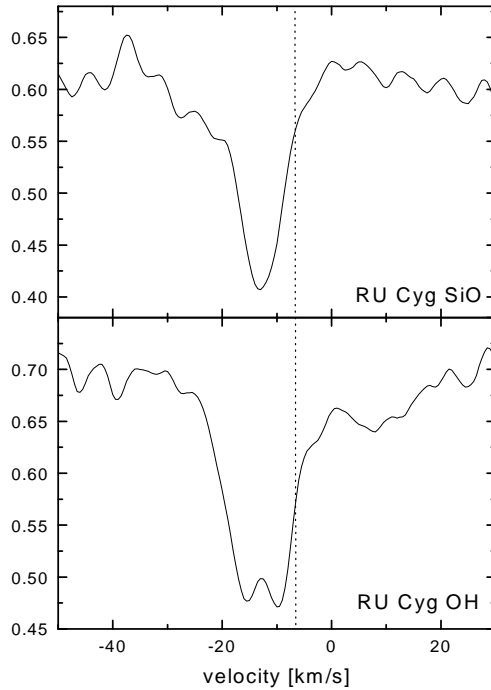


**Fig. 12.** SiO (upper panel) and OH (lower panel) line profiles of RU Cyg. The dotted line marks the systemic velocity.

H<sub>2</sub>O is detectable in three of the SR stars, RX Boo, g Her, and SW Vir. In all three it is seen in emission. In SW Vir the H<sub>2</sub>O line has an inverse P Cyg shape with absorption at  $-18.4 \text{ km s}^{-1}$  and emission at  $-11.3 \text{ km s}^{-1}$

heliocentric. The H<sub>2</sub>O velocity for RX Boo is  $-11.3 \text{ km s}^{-1}$  and  $+6.8 \text{ km s}^{-1}$  for g Her (heliocentric). Comparison with center of mass velocities from radio observations shows that the water emission occurs always close to but not necessarily exactly at the systemic velocity of the star. The largest difference was found for g Her (CO radio velocity:  $+1.3 \text{ km s}^{-1}$ ).

## 7. Conclusions

### 7.1. Explaining low resolution spectra

Considerable variations in the strengths of SiO bands during a light cycle have been observed in low resolution spectra of AGB stars. In our high resolution observations the lines are convincingly present at all phases, showing a presence of SiO in the atmosphere throughout the light cycle. Therefore it is obvious that the simplest proposals, e.g. the dissociation of a large fraction of molecules near maximum light, do not explain the spectrum. This has been suggested to explain the extreme weakening of the SiO bands near light maximum observed in low resolution spectra (e.g. Rinsland & Wing 1982). The identification of emission components in these lines suggests the blending and cancellation of absorption and emission as the explanation for the weakening (Bessell et al. 1996, Aringer et al. 1999b). It is interesting to note that Aringer et al. (2000) found a significant emission in 4  $\mu\text{m}$  range of ISO SWS spectra of RCas, which they attributed to SiO, while we found only a rather inconspicuous emission component in our high resolution spectra. This discrepancy suggests strong cycle-to-cycle variations which warrant further investigation.

### 7.2. Dynamics of miras

A surprise in the 4  $\mu\text{m}$  spectra is the large degree of combination of velocity variations that arise close to the pulsation driving zone with grossly non-periodic variations arising in extended atmospheric layers. In general the continuous opacity in the 4  $\mu\text{m}$  region is significantly higher than in the 1.6  $\mu\text{m}$  range. As a consequence there is a tendency for lines to originate further out. Therefore many molecular features seen at 4  $\mu\text{m}$  monitor stellar variability in the outer parts of the atmosphere, especially many SiO and H<sub>2</sub>O lines. A similar increase in the continuous opacity toward the blue is well documented and seen in the appearance of the visual spectrum. The line profile variations seen at 4  $\mu\text{m}$  appear similar to those found for K I and Fe I lines around 8000 Å by Gillet et al. (1985). Part of the periodic and non-periodic variations seen in the 4  $\mu\text{m}$  region could also be due to a deviation from spherical symmetry.

The four stars in our sample show both strong similarities and differences in the 4  $\mu\text{m}$  lines. Especially for RCas we find a quite different behavior for most of the

lines. We conclude that, while the lower regions of the atmosphere where pulsation originates are very similar in all the miras, the outer layers of the mira atmosphere are much more distinctive. This could be the result of evolutionary state along the AGB as might be suggested by the range of periods. Other possibilities are differences in the fundamental properties like mass, metallicity, or C/O. Or the behavior is unique for each star resulting from spatial inhomogeneities in the atmosphere. Our sample is too small to differentiate between these possibilities. However we note that R Leo and o Cet have a similar period and similar C/O (based on the water and CO line strengths) and have more similarity in their 4  $\mu\text{m}$  spectra than with the other two miras.  $\chi$  Cyg, although having a similar period to R Cas, is an S-type star so differences between the line profiles in these stars are expected to be produced by the different atmospheric structure which is related to chemical composition.

Fig. 9 shows, that the lines can be a tracer of the pulsation, like those in the 1.6  $\mu\text{m}$  spectrum, but that in some cycles irregular behavior occurs. Periodicities in the outer layers different from the photometric period have been suggested from dynamical model atmospheres (see e.g. Fig. 1 in Höfner & Dorfi 1997, and Hofmann et al. 1998). The observational findings can be qualitatively understood in the framework of these dynamical models of AGB star atmospheres. During some cycles, which seem to be marked by a brighter visual maximum, part of the outward moving layers decelerates less than in other cycles due to a smaller density in the outer layers. This density variation may be related to a non continuous mass loss. Such deviations are not monitored by lines formed deeper inside the atmosphere. It is therefore an effect only occurring in the outer parts of the star. This means that this behavior is not related to a different strength of the pulsation.

In this context it is interesting to note, that Rinsland & Wing (1982) made two low resolution 4  $\mu\text{m}$  spectra of each of the miras R Cyg,  $\chi$  Cyg and R Cas separated by almost exactly one light cycle. In two miras, R Cas and  $\chi$  Cyg, they detected a clear difference in the overall strength of the SiO (2,0) and (3,1) bands between the two observations made at similar phase. This is in good agreement with the findings discussed above.

### 7.3. SRVs

Small amplitude variables like the SRVs of our sample are thought to be more compact than miras. Variations of CO lines at 1.6  $\mu\text{m}$  (Hinkle et al. 1997, Lebzelter 1999) indicate that SRVs vary with a much smaller velocity amplitude and that shock fronts are very weak or do not occur at all. In agreement with this finding, the SRVs of our sample do not show such extreme emission components as found in miras. The line profiles of most SRVs show a similar shape and strength. This indicates that their outer atmospheric

layers show a similar structure. Due to the lack of time series for these stars no study on their individual variability is possible.

As our main result for SRVs we note that both the occurrence of emission components as well as the asymmetries and the shifts relative to the center of mass velocity clearly indicate that velocity fields have to be included into a model atmosphere to reproduce the results properly. Hydrostatic models cannot be used for high resolution spectra of these stars. However, the fact that the effects of the stellar pulsation are still rather small in SRVs compared to miras makes these stars excellent starting points for adapting dynamical models to the observations.

## 8. Outlook

The aim of this paper was to present and to discuss qualitatively the observational results of our high resolution spectroscopic monitoring of AGB variables. In a forthcoming paper we will present synthetic spectra based on dynamic model atmospheres in order to model the observations presented here.

However, an obvious explanation of the non-regular variations is inhomogeneities in the upper atmosphere. These inhomogeneities could be in the form of filaments or clouds in the extended stellar atmosphere. Unique filament structure would explain non-cyclic behavior and the strong spectral identity of individual stars. There is considerable evidence from maser observations of such condensations in the outer atmosphere. The SiO maser, which is probably formed in the same atmospheric region as some of the 4  $\mu\text{m}$  lines, is clearly formed in condensations (Diamond et al. 1994). Large scale inhomogeneities are indicated by maps and images of AGB circumstellar shells. A further indication for inhomogeneities in the atmospheres of AGB stars come from polarimetry measurements. As shown from model calculation (Harrington 1969) observational results can be understood if it is assumed that temperature variations occur over the stellar surface. This model has been applied successfully to observations of o Cet by Tomaszewski et al. (1980). Such filament structures currently exceed foreseeable modeling capabilities, but it might be possible to include their effects in future dynamical model atmospheres.

*Acknowledgements.* We wish to thank Dr. Susanne Höfner for fruitful discussions on her model atmospheres. This work was supported by Austrian Science Fund Projects S7308-AST and P14365-PHY. K.H.H. would like to thank the NOAO director Dr. Sidney Wolff for funding two visits to the Institut für Astronomie which made this research possible. K.H.H. would also like to acknowledge the hospitality of Drs. Michel Breger and Josef Hron at the Institut für Astronomie in Vienna. This research made use of the SIMBAD database operated by CDS in Strasbourg, France, and NASA's Astrophysics Data System Bibliographic Services. In this research, we have used, and acknowledge with thanks, data from the AAVSO International

Database, based on observations submitted to the AAVSO by variable star observers worldwide.

## References

- Alvarez R., Lancon A., Plez B., Wood P.R., 2000, *A&A* 353, 322
- Aringer B., Jørgensen U.G., Langhoff S.R., 1997, *A&A* 323, 202
- Aringer B., Kerschbaum F., Hron J., et al., 1999a, in: *Asymptotic Giant Branch Stars*, IAU Symp. 191, eds. T. Le Bertre, A. Lebre & C. Waelkens, Astronomical Society of the Pacific
- Aringer B., Höfner S., Wiedemann G., et al., 1999b, *A&A* 342, 799
- Aringer B., 2000, PhD thesis, University of Vienna
- Aringer B., Kerschbaum F., Hron J., Höfner S., 2000, in: (ed.), *Proc. "ISO beyond the Peaks"*, ed. A. Salama, ESA-SP 456, 3
- Beer R., Lambert D.L., Sneden C., 1974, *PASP* 86, 806
- Bessell M.S., Scholz M., Wood P.R., 1996, *A&A* 307, 481
- Le Blanc R.B., White, J.B., Bernath P.F., 1994, *J. Mol. Spec.* 164, 574
- Benson P.J., Little-Marenin I., Woods T.C., et al., 1990, *ApJS* 74, 911
- Colomer F., Reid M.J., Menten K.M., Bujarrabal V., 2000, *A&A* 355, 979
- Coxon J.A., 1980, *Canad. J. Phys.* 58 933
- Coxon J.A., Foster S.C., 1982, *Canad. J. Phys.* 60, 41
- Diamond, P.J., Kemball, A.J., Junor, W., Zensus, A., Benson, J., & Dhawan, V., 1994, *ApJ* 430 L61
- Gail H.P., Sedlmayr E., 1986, *A&A* 166, 225
- Gillet D., Maurice E., Bouchet P., Ferlet R., 1985, *A&A* 148, 155
- Habing H.J., 1996, *A&A Rv* 7, 97
- Hall D.N.B., Ridgway S.T., Bell E.A., Yarborough J.M., 1979, *Proc. SPIE* 172, 121
- Harrington J.P., *Astrophysical Letters* 3, 165
- Hinkle K.H. 1978, *ApJ* 220, 210
- Hinkle K.H., Barnes T.G., 1979, *ApJ* 227, 923
- Hinkle K.H., Barnes T.G., Lambert D.L., Beer R., 1976, *ApJ* 210, L141
- Hinkle K.H., Hall D.N.B., Ridgway S.T., 1982, *ApJ* 252, 697
- Hinkle K.H., Scharlach W.W.G., Hall D.N.B., 1984, *ApJS* 56, 1 [HSH]
- Hinkle K.H., Wallace L., Livingston, W., 1995, *Infrared Atlas of the Arcturus Spectrum, 0.9-5.3 microns* (San Francisco:ASP)
- Hinkle K.H., Lebzelter, T., Scharlach W.W.G., 1997, *AJ* 114, 2686
- Hinkle K.H., Aringer B., Lebzelter T., Martin C.L., Ridgway S.T., 2000, *A&A* 363, 1065
- Höfner S., 1999, *A&A* 346, L9
- Höfner S., Dorfi E.A., 1997, *A&A* 319, 648
- Höfner S., Jørgensen U.G., Loidl R., Aringer B., 1998, *A&A* 340, 497
- Hofmann K.-H., Scholz M., Wood P.R., 1998, *A&A* 339, 846
- Jewell P.R., Snyder L.E., Walmsley C.M., Wilson T.L., Genesheimer P.D., 1991, *A&A* 242, 211
- Johnson H.L., Mendez M.E., 1970, *AJ* 75, 785
- Kerschbaum F., Olofsson H., 1999, *A&AS* 138, 299
- Kholopov P.N., Samus N.N., Frolov M.S., et al., 1985–88, *General Catalogue of Variable Stars*, 4<sup>th</sup> edition, "Nauka" Publishing House, Moscow (GCVS4)
- Lebzelter T., 1999, *A&A* 351, 644
- Matsuura M., Yamamura I., Murakami H., et al., 1999, *A&A* 348, 579
- Mattei J.A., 1984–95, *AAVSO Bulletin* 47–58
- Mattei J.A., 2000, *Observations from the AAVSO International Database*, private communication
- Menten K.M., Melnick G.J., 1989, *ApJ* 341, L91
- Menten K.M., Young K., 1995, *ApJ* 450, L67
- Merrill P.W., 1946, *ApJ* 103, 275
- Ridgway S.T., Carbon D.F., Hall D.N.B., Jewell J., 1984, *ApJS* 54, 177
- Rinsland C.P., Wing R.F., 1982, *ApJ* 262, 201
- Ryde N., Gustafsson B., Eriksson K., Hinkle K., 2000, *ApJ* 545, 945
- Spinrad H., Wing R.F., 1969, *ARA&A* 7, 249
- Tomaszewski L., Landstreet J.D., McLean I.S., Coyne G.V., 1980, *ApJ* 238, 935
- Truong-Bach, Sylvester R.J., Barlow M.J., et al., 1999, *A&A* 345, 925
- Tsuji T., 2000 *ApJ* 540, L99
- Tsuji T., Ohnaka K., Aoki W., Yamamura I., 1997, *A&A* 320, L1
- Wallerstein G., 1985, *PASP* 97, 994
- Willson L.A., Bowen G.H., 1986, in: Zeilik M., Gibson D.M. (eds.): *Lecture Notes in Physics Vol. 254, Cool Stars, Stellar Systems and the Sun*, p. 385
- Winters J.M., Le Bertre T., Jeong K.S., Helling Ch., Sedlmayr E., 2000, *A&A* 361, 641
- Yamamura I., de Jong T., Cami J., 1999, *A&A* 348, L55
- Zobov N. F., Polyansky, O. L., Tennyson, J., Shirin, S. V., Nassar, R., Hirao, T., Imajo, T., Bernath, P. F., Wallace, L. 2000, *ApJ* 530, 994